Original Article

Heterogeneity of fibroblast activation protein expression in the microenvironment of an intracranial tumor cohort: head-to-head comparison of gallium-68 FAP inhibitor-04 (^{68}Ga-FAPi-04) and fluoride-18 fluoroethyl-L-tyrosine (^{18}F-FET) in positron emission tomography-computed tomography imaging

Tao Hua[1#], Mingyu Chen[2,3,4,5,6#], Pengfei Fu[2,3,4,5,6], Weiyan Zhou[1], Wen Zhao[7], Ming Li[1], Chuantao Zuo[1], Yihui Guan[1], Hongzhi Xu[2,3,4,5,6]

[1]Department of Nuclear Medicine & Positron Emission Tomography Center, Huashan Hospital, Fudan University, Shanghai, China; [2]Department of Neurosurgery, Huashan Hospital, Shanghai Medical College, Fudan University, Shanghai, China; [3]National Center for Neurological Disorders, Shanghai, China; [4]Shanghai Key Laboratory of Brain Function and Restoration and Neural Regeneration, Shanghai, China; [5]Neurosurgical Institute of Fudan University, Shanghai, China; [6]Shanghai Clinical Medical Center of Neurosurgery, Shanghai, China; [7]Department of Anesthesiology, Huashan Hospital, Fudan University, Shanghai, China

Contributions: (I) Conception and design: T Hua, H Xu; (II) Administrative support: C Zuo, Y Guan; (III) Provision of study materials or patients: M Chen, P Fu, W Zhao, M Li; (IV) Collection and assembly of data: T Hua, M Chen, P Fu, W Zhao, M Li; (V) Data analysis and interpretation: T Hua, M Chen, W Zhou; (VI) Manuscript writing: All authors; (VII) Final approval of manuscript: All authors.

[#]These authors contributed equally to this work.

Correspondence to: Hongzhi Xu, MD. Department of Neurosurgery, Huashan Hospital, Shanghai Medical College, Fudan University, 12 Middle Wulumuqi Rd., Shanghai 200040, China; National Center for Neurological Disorders, Shanghai, China; Shanghai Key Laboratory of Brain Function and Restoration and Neural Regeneration, Shanghai, China; Neurosurgical Institute of Fudan University, Shanghai, China; Shanghai Clinical Medical Center of Neurosurgery, Shanghai, China. Email: xuhongzhi95@sina.com.

Background: Cancer-associated fibroblasts (CAFs) within the tumor microenvironment (TME) can interact with tumor parenchymal cells to promote tumor growth and migration. Fibroblast activation protein (FAP) expressed by CAFs can be targeted with positron emission tomography (PET) tracers, but studies on FAP expression patterns in intracranial tumors remain scarce. We aimed to evaluate FAP expression patterns in intracranial tumors with gallium-68 FAP inhibitor-04 (^{68}Ga-FAPi-04) and immunohistochemical staining and to observe the interactions between CAFs and tumor cells with a head-to-head comparison of ^{68}Ga-FAPi-04 and fluoride-18 fluoroethyl-L-tyrosine (^{18}F-FET) for PET quantification analysis.

Methods: We prospectively enrolled 22 adult patients with intracranial mass lesions. ^{68}Ga-FAPi-04 and ^{18}F-FET PET-computed tomography (PET/CT) brain imaging were applied before surgery. Maximal tumor-to-brain ratio (TBRmax), metabolic tumor volume (MTV), and total lesion tracer uptake (TLU) was obtained, and different thresholds were used for ^{68}Ga-FAPi-04-positive lesion delineation owing to the lack of relevant guidelines. The MTV and TLU ratios of both tracers were calculated. Linear regression was applied to observe the differential efficacy of semiquantitative PET parameters.

Results: A total of 22 patients with a mean age of 50±13 years (range, 27–69 years) were enrolled. Heterogeneous patterns of ^{68}Ga-FAPi-04 uptake [median of maximal standardized uptake value (SUVmax) =3.8; range, 0.1–19.1] were found. More malignant tumors, including brain metastasis, glioblastoma, and medulloblastoma, generally exhibited more significant ^{68}Ga-FAPi-04 uptake than did the less malignant tumors, while the SUVmax and TBRmax exhibited nonsignificant differences across three intracranial lesion groups of

primary brain tumor, brain metastasis, and noncancerous disease (SUVmax: P=0.092; TBRmax: P=0.189). Immunohistochemistry staining showed different stromal FAP expression status in various intracranial lesions. In 15 patients with positive ^{68}Ga-FAPi-04 intracranial tumor uptake, the MTV_{FAPi}:MTV_{FET} ratio had differential efficacy in various types of intracranial tumors [95% confidence interval (CI): 0.572–7.712; P=0.027], and further quantification analyses confirmed the differential ability of the MTV_{FAPi}:MTV_{FET} ratio (95% CI: −0.045 to 11.013, P=0.052; 95% CI: 0.044–17.903, P=0.049; 95% CI: −1.131 to 30.596, P=0.065) with different isocontour volumetric thresholds.

Conclusions: This head-to-head study demonstrated heterogeneous FAP expression in intracranial tumors. The FAP expression volume percentage in tumor parenchyma may therefore offer benefit with respect to differentiating between intracranial tumor types.

Keywords: Cancer-associated fibroblasts (CAFs); fibroblast activation protein (FAP); tumor microenvironment (TME); fibroblast activation protein inhibitor (FAPi); positron emission tomography (PET)

Submitted Jan 15, 2024. Accepted for publication May 14, 2024. Published online Jun 27, 2024.
doi: 10.21037/qims-24-82
View this article at: https://dx.doi.org/10.21037/qims-24-82

Introduction

Intracranial tumors exhibit substantial heterogeneity, which could be attributed to both tumor parenchymal cells and benign cells in the tumor microenvironment (TME). Gliomas, the most common central nervous system tumors, exemplify this, demonstrating pronounced intratumoral and intertumoral heterogeneity (1-3). Interactions between glioma cells and adjacent TME cells in the tumor stroma occur through various mechanisms, promoting tumor pathophysiological behaviors such as proliferation, migration, and angiogenesis (4,5).

Positron emission tomography (PET) imaging with radio-labeled amino acid tracers such as fluoride-18 fluoroethyl-L-tyrosine (^{18}F-FET) can contribute to brain tumor grading, differential diagnosis, prognostication, treatment planning, and monitoring (6-8). The Response Assessment in Neuro-Oncology (RANO) working group endorses this imaging modality as a valuable complement to magnetic resonance imaging (MRI) in all stages of glioma management (9). Although these radio-labeled amino acid tracers have appreciable efficacy, they primarily target L-type amino acid transporters (LATs), which are transmembrane proteins expressed in tumor cells (10,11).

Cancer-associated fibroblasts (CAFs), capable of secreting growth factors and inflammatory cytokines, are critically involved in the interactions between tumor cells and stromal cells (12,13). Fibroblast activation protein (FAP), a transmembrane glycoprotein, may be overexpressed by CAFs in the TME (14,15). Radio-labeled fibroblast activation protein inhibitors (FAPis) have demonstrated efficacy in imaging CAFs activities across a range of solid tumors with satisfactory results.

As there is significant FAP accumulation in the stroma of malignant tumors and satisfactory tissue contrast, FAP-targeted imaging has efficacy in malignant tumor detection, tumor delineation, metastatic lymph node recognition, tumor staging and restaging, and radiotherapy planning (16-18). Research suggests that FAP-targeted imaging can influence the treatment decisions after the detection of extra-lymph node metastasis in breast carcinomas (19). FAPi imaging also aids in the differentiation of malignant transformation of pancreatic intraductal papillary mucinous neoplasms (20). While there is some evidence indicating that certain types of gliomas overexpress FAP (21), data on the FAP expression in other intracranial tumors have not been well established in the literature and should be pursued further. Moreover, the correlation between the volume of FAP in the TME and tumor malignancy degree in various intracranial tumors is of considerable interest.

This prospective, head-to-head study applied gallium-68 FAPi-04 (^{68}Ga-FAPi-04) and ^{18}F-FET PET-computed tomography (CT) imaging to patients with intracranial tumors before surgery to investigate the spectrum of FAP expression. Immunohistochemical staining was used to examine the patterns of FAP expression. A quantification analysis of PET parameters was employed to characterize the relationship between FAP expression volume in tumor

stroma and the degree of malignancy.

Methods

Ethical approval

This study was conducted according to the Declaration of Helsinki (as revised in 2013). Ethical approval of our previously written study protocol and consequent analytical design was obtained from Ethics Committee of Huashan Hospital, Fudan University (No. 2021-891), and informed consent was obtained from all individual participants. The study protocol was not registered on a public platform and did not involve any interventional procedures.

Study design

Adult preoperative patients with intracranial mass lesions were enrolled. Anatomic MRI after symptom occurrence was collected and reviewed for initial diagnosis by outpatient neurosurgeons in Huashan Hospital before admission for further investigation and treatment. Those patients who had already received treatment including surgery, radiosurgery, radiotherapy, or chemotherapy were excluded from the study. Enrolled adult patients with intracranial tumors received ^{68}Ga-FAPi-04 and ^{18}F-FET PET/CT brain imaging before surgery from October 2022 to March 2023 in the Neurosurgery Department of Huashan Hospital, Fudan University. Semiquantitative imaging parameters and immunohistochemical staining were obtained for diagnostic evaluation of this head-to-head study. Written informed consent from patients for dual-tracer PET/CT imaging and follow-up analysis was obtained.

Imaging protocols

^{68}Ga-FAPi-04 and ^{18}F-FET tracers were synthesized in the Department of Nuclear Medicine & PET Center of Huashan Hospital, Fudan University.

For ^{18}F-FET PET/CT imaging, patients fasted for a minimum of 4 hours prior to imaging. A 20-minute static scan was conducted in 3-dimensional (3D) mode with a Biograph mCT Flow Edge 128 PET/CT system (Siemens Healthineers, Erlangen, Germany) 20 minutes after intravenous bolus injection of ^{18}F-FET (185±17.0 MBq). Attenuation correction was performed using low-dose CT (tube current =150 mAs, voltage =120 kV, acquisition =64×0.6 mm, convolution kernel = H30s, slice thickness =5 mm, interslice gap = 1.5 mm) prior to the emission scan. Postacquisition, PET images were reconstructed using the ordered subset expectation maximization (OSEM) algorithm with a Gaussian filter and a full width at half maximum of 3.5 mm at the center of the field of view.

In ^{68}Ga-FAPi-04 PET/CT imaging, 30 minutes after intravenous bolus injection of ^{68}Ga-FAPi-04 (185±29.2 MBq), a 30-minute static scan was conducted in 3D mode with a uMI510 PET/CT (United Imaging, Shanghai, China). Attenuation correction was similarly performed using low-dose CT prior to the emission scan. PET images were also reconstructed using the OSEM algorithm with a Gaussian filter and the same full width at half maximum after acquisition.

Image analysis

PET/CT images were analyzed with a syngo.via workstation (Siemens Healthineers). Two experienced nuclear medicine physicians (W.Z. and T.H., with over 6 and 13 years of experience, respectively) performed blinded ^{68}Ga-FAPi-04 and ^{18}F-FET PET/CT positive lesion judgement and lesion delineation before surgical treatment.

Structural MRI was initially read before PET/CT lesion delineation. For ^{18}F-FET PET/CT imaging, mean standardized uptake value (SUVmean) of the brain background was measured in a crescent-shaped area, encompassing both gray and white matter on the lesion's contralateral hemisphere. Subsequently 1.6 times of background SUVmean was used for lesion delineation, and the maximal standardized uptake value (SUVmax), metabolic tumor volume (MTV), and total lesion tracer uptake (TLU) were obtained. Maximal tumor-to-brain ratio (TBRmax) was calculated by dividing the intracranial lesion SUVmax with the background SUVmean.

For ^{68}Ga-FAPi-04 imaging, the background SUVmean was measured similarly to that of ^{18}F-FET PET. Lesion SUVmax and TBRmax were measured. Due to the lack of guidelines for a FAPi-positive lesion delineation and extremely low uptake of the brain background, a series of isocontour volumetric thresholds including 20%, 30%, 40%, and 50% of lesion SUVmax were measured for MTV_{FAPi} and TLU_{FAPi} measurements. Different MTV_{FAPi}:MTV_{FET} and TLU_{FAPi}:TLU_{FET} ratios were calculated for further analysis.

Histological analysis

Pathological diagnosis was completed in the Pathology

Department of Huashan Hospital, Fudan University. Characteristic surgical resection slices were selected for FAP immunohistochemistry staining as per the FAP kit instruction (Abcam, Cambridge, UK). Briefly, heat-mediated antigen retrieval with buffer was applied before FAP immunohistochemical staining. Tissue sections were incubated at 4 ℃ overnight with a 1:250 anti-fibroblast activation antibody (RRID: AB_207178; Abcam, Cambridge, UK). Streptavidin-biotin complex was used for incubation before staining and visualization.

FAP immunohistochemical staining scores were assigned by two independent pathologists who were blinded to patients' clinical and PET/CT imaging analysis results. The scoring method was applied as previously described (22), with 0 indicating complete absence or very minimal FAP staining in less than 1% of the evaluation area, 1 indicating weak FAP immunohistochemical staining from 1% to 10% of the evaluation area, 2 indicating moderate FAP immunohistochemical staining from 11% to 50% of the evaluation area, and 3 indicating strong FAP immunohistochemical staining over 50% of the evaluation area.

Statistical analysis

Descriptive statistics are expressed as the mean and standard deviation or median and range. The *t*-test and one way analysis of variance was used to compare continuous variables. The Wilcoxon signed rank or Kruskal-Wallis test was performed if a normal distribution of variables was not met. Linear regression analysis was applied to investigate the relationship of pathological diagnosis and PET parameters. The variance inflation factor was used to control multicollinearity. Intraclass correlation coefficients (ICCs) for PET parameter measurements and FAP immunohistochemical scoring were assessed, and the results were classified as poor (less than 0.2), fair (0.21–0.4), moderate (0.41–0.6), good (0.61–0.8), and very good (0.8–1.0). All statistical analyses were performed with Stata version 17 (College Station, TX, USA). In all analyses, $P<0.05$ was considered to indicate a statistically significant difference.

Results

Patients characteristics

This study enrolled 22 patients, including 14 men and 8 women, with a mean age of 50±13 years (range, 27–69 years). Consecutive ^{68}Ga-FAPi-04 and ^{18}F-FET PET/CT imaging scans were applied with an at least a 24-hour interval for each patient in our cohort. Surgical treatment was performed after dual-tracer PET/CT within 8 days and included 20 surgical resections and 2 stereotactic biopsies. Primary brain tumor, brain metastasis, and noncancerous disease were observed. Eight specific histological diagnoses were identified according to the 2021 World Health Organization (WHO) Classification of Tumors of the Central Nervous System, which included WHO grade 4 glioblastoma isocitrate dehydrogenase wild type (IDH-wt), metastatic carcinoma, oligodendroglioma, WHO grade 2 IDH mutation (IDH-mu) and 1p/19q codeleted, noncancerous lesions, WHO grade 4 astrocytoma IDH-mu, WHO grade 3 astrocytoma IDH-mu, WHO grade 4 medulloblastoma not otherwise specified (NOS), and WHO grade 1 ganglioglioma. Demographic details of the cohort are provided in *Table 1*.

Comparison of two tracers in PET imaging of lesions

A total of 32 intracranial lesions were observed in the 22 ^{18}F-FET PET images, including in 5 patients with multiple lesions; meanwhile, 18 lesions were observed in 16 ^{68}Ga-FAPi-04 PET images. In 1 case of glioblastoma (No. 6), ^{18}F-FET PET showed 4 lesions while ^{68}Ga-FAPi-04 PET showed 2. In 1 case of WHO grade 4 astrocytoma IDH-mu (No. 5), ^{18}F-FET PET showed 4 lesions while ^{68}Ga-FAPi-04 PET showed 1. In one case of brain metastasis (No. 2), ^{18}F-FET PET showed 2 lesions while ^{68}Ga-FAPi-04 PET showed 1. In another case of brain metastasis (No. 16), both PET tracers showed 2 lesions. In 1 case of noncancerous disease (No. 10), ^{18}F-FET PET showed 3 lesions but ^{68}Ga-FAPi-04 PET showed none. The difference in detection between the tracers in PET was significant ($P=0.046$).

Analysis of patient-based PET semiquantitative parameters

ICCs showed very good agreement between the different tracers for ^{18}F-FET and ^{68}Ga-FAPi-04 PET/CT parameter measurements (ICC >0.95, $P<0.001$; ICC >0.87, $P<0.001$), and the results of reader one (W.Z.) were used for analysis.

For ^{68}Ga-FAPi-04 PET images, brain metastasis showed highest uptake. The lesion median SUVmax and TBRmax were 4.8 (range, 4.5–19.1) and 161.0 (range, 148.7–382.2), respectively. In primary brain tumors, FAPi uptake in

Table 1 Demographic characteristics of the patient cohort

Patient No.	Age (years)	Sex	Location	Treatment	Pathology	WHO grade	FAP score
1	56	M	Parietal-temporal left	TR	Glioblastoma, IDH-wt	4	2
2	35	M	Temporal right	TR	Metastatic carcinoma	N/A	2
3	69	F	Parietal left	TR	Glioblastoma, IDH-wt	4	3
4	69	M	Frontal-parietal right	TR	Glioblastoma, IDH-wt	4	1
5	52	M	Frontal bilateral and corpus callosum	SB	Astrocytoma, IDH-mu	4	1
6	55	M	Temporal left	TR	Glioblastoma, IDH-wt	4	2
7	58	M	Temporal left	TR	Glioblastoma, IDH-wt	4	2
8	37	F	Temporal left	TR	Glioblastoma, IDH-wt	4	2
9	48	M	Frontal-temporal-insular left	TR	Glioblastoma, IDH-wt	4	2
10	27	M	Temporal and thalamus bilateral	SB	Gliosis	N/A	1
11	29	M	Temporal left	SR	Astrocytoma, IDH-mu	3	1
12	58	F	Occipital left	TR	Glioblastoma, IDH-wt	4	2
13	46	M	Frontal right	TR	Multifocal encephalomalacia	N/A	2
14	49	F	Frontal right	TR	Oligodendroglioma	2	1
15	58	M	Frontal-parietal right	TR	Metastatic carcinoma	N/A	3
16	64	F	Occipital left	TR	Metastatic carcinoma	N/A	3
17	54	M	Frontal right	TR	Glioblastoma, IDH-wt	4	2
18	35	F	Frontal-temporal-insular right	TR	Oligodendroglioma	2	1
19	59	F	Frontal left	TR	Oligodendroglioma	2	1
20	42	F	Temporal right	TR	Ganglioglioma	1	0
21	35	M	Cerebellum right	TR	Medulloblastoma, NOS	4	1
22	66	M	Frontal-parietal right	TR	Glioblastoma, IDH-wt	4	3

WHO, World Health Organization; FAP, fibroblast activation protein; M, male; F, female; TR, total resection; IDH, isocitrate dehydrogenase; wt, wild type; N/A, non-applicable; SB, stereotactic biopsy; mu, mutant; SR, subtotal resection; NOS, not otherwise specified.

WHO grade 4 glioblastoma IDH-wt was the most obvious, and the lesion median SUVmax and TBRmax were 4.2 (range, 0.2–11.7) and 126.8 (range, 5.3–389.0), respectively. In noncancerous lesions, the median SUVmax and TBRmax were 2.2 (range, 0.3–4.0) and 57.4 (range, 14.5–100.3), respectively. The brain background median SUVmean was 0.03 (range, 0.02–0.06). There were no significant differences in intracranial lesion types, including brain metastasis, primary brain tumor, and noncancerous disease, in terms of SUVmax-FAPi (P=0.092) or TBRmax-FAPi (P=0.189); there were similarly no significant differences among specific histological diagnoses (SUVmax-FAPi: P=0.212; TBRmax-FAPi: P=0.132).

For ^{18}F-FET PET imaging, the highest tracer uptake was present in primary brain tumors, and the median SUVmax and TBRmax were 3.5 (range, 1.6–6.3) and 4.4 (range, 2.1–5.9), respectively. In brain metastasis, the median SUVmax and TBRmax were 2.7 (range, 2.5–3.7) and 3.6 (range, 2.8–4.2), respectively. In noncancerous patients, the median SUVmax and TBRmax were 3.0 (range, 2.2–3.8) and 4.4 (range, 2.7–6.1), respectively. There were no significant differences between the three intracranial lesion types in terms of SUVmax-FET (P=0.648) or TBRmax-FET (P=0.709); there were similarly no significant differences among specific histological diagnoses (SUVmax-FET: P=0.644; TBRmax-FET: P=0.553).

We found no evidence of differences in patient-based SUVmax between the PET images of the different tracers

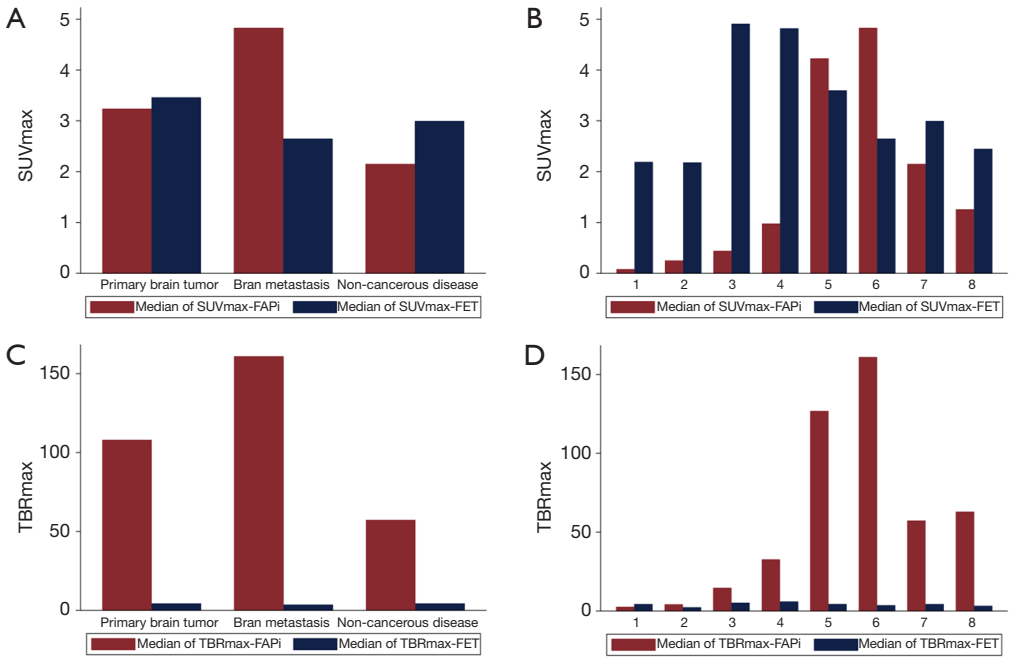

Figure 1 Comparison of the median SUVmax and TBRmax of ^{68}Ga-FAPi-04 and ^{18}F-FET uptake in intracranial lesions. 1: ganglioglioma; 2: oligodendroglioma; 3: grade 3 astrocytoma IDH-mu; 4: grade 4 astrocytoma IDH-mu; 5: grade 4 glioblastoma IDH-wt; 6: metastatic carcinoma; 7: noncancerous disease; 8: medulloblastoma. SUVmax, maximal standardized uptake value; FAPi, fibroblast activation protein inhibitor; FET, fluoroethyl-L-tyrosine; TBRmax, maximal tumor-to-brain ratio; ^{68}Ga-FAPi-04, gallium-68 fibroblast activation protein inhibitor 04; ^{18}F-FET, fluoride-18 fluoroethyl-L-tyrosine; IDH, isocitrate dehydrogenase; wt, wild type; mu, mutant.

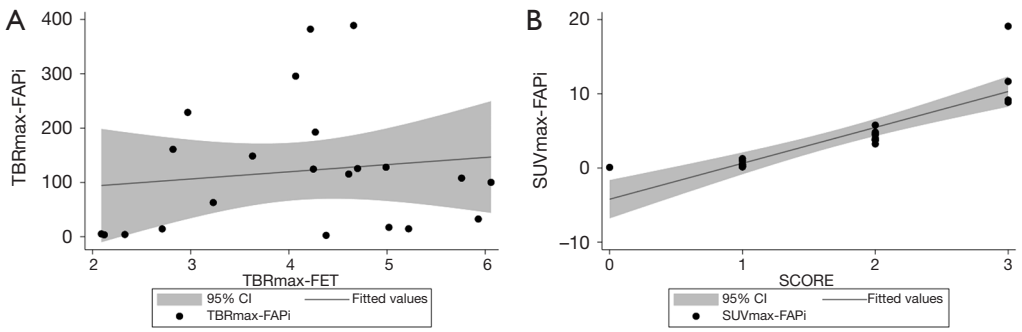

Figure 2 Scatter plot and regression plot of lesion tracer uptake and immunohistochemical score. (A) Scatter plot and regression plot of participants' dual-tracer TBRmax with ^{68}Ga-FAPi-04 and ^{18}F-FET PET images. (B) Scatter plot and regression plot of participants' ^{68}Ga-FAPi-04 uptake SUVmax and FAP immunohistochemical staining score. TBRmax, maximal tumor-to-brain ratio; FAPi, fibroblast activation protein inhibitor; FET, fluoroethyl-L-tyrosine; CI, confidence interval; FAP, fibroblast activation protein; SUVmax, maximal standardized uptake value; ^{68}Ga-FAPi-04, gallium-68 fibroblast activation protein inhibitor 04; ^{18}F-FET, fluoride-18 fluoroethyl-L-tyrosine; PET, positron emission tomography.

(FAPi: 4.15±4.66; FET 3.42±1.19; P=0.935), while the TBRmax of FAPi was significantly higher than that of FET (FAPi: 120.83±117.47; FET 4.09±1.21; P=0.0001). The comparisons are provided in *Figure 1*, the scatter plot of the TBRmax uptake in lesions with both tracers is shown in *Figure 2*, and illustrative cases are provided in *Figure 3*.

Out of the 16 ^{68}Ga-FAPi-04-positive patients, 15 surgically treated intracranial tumors were used to

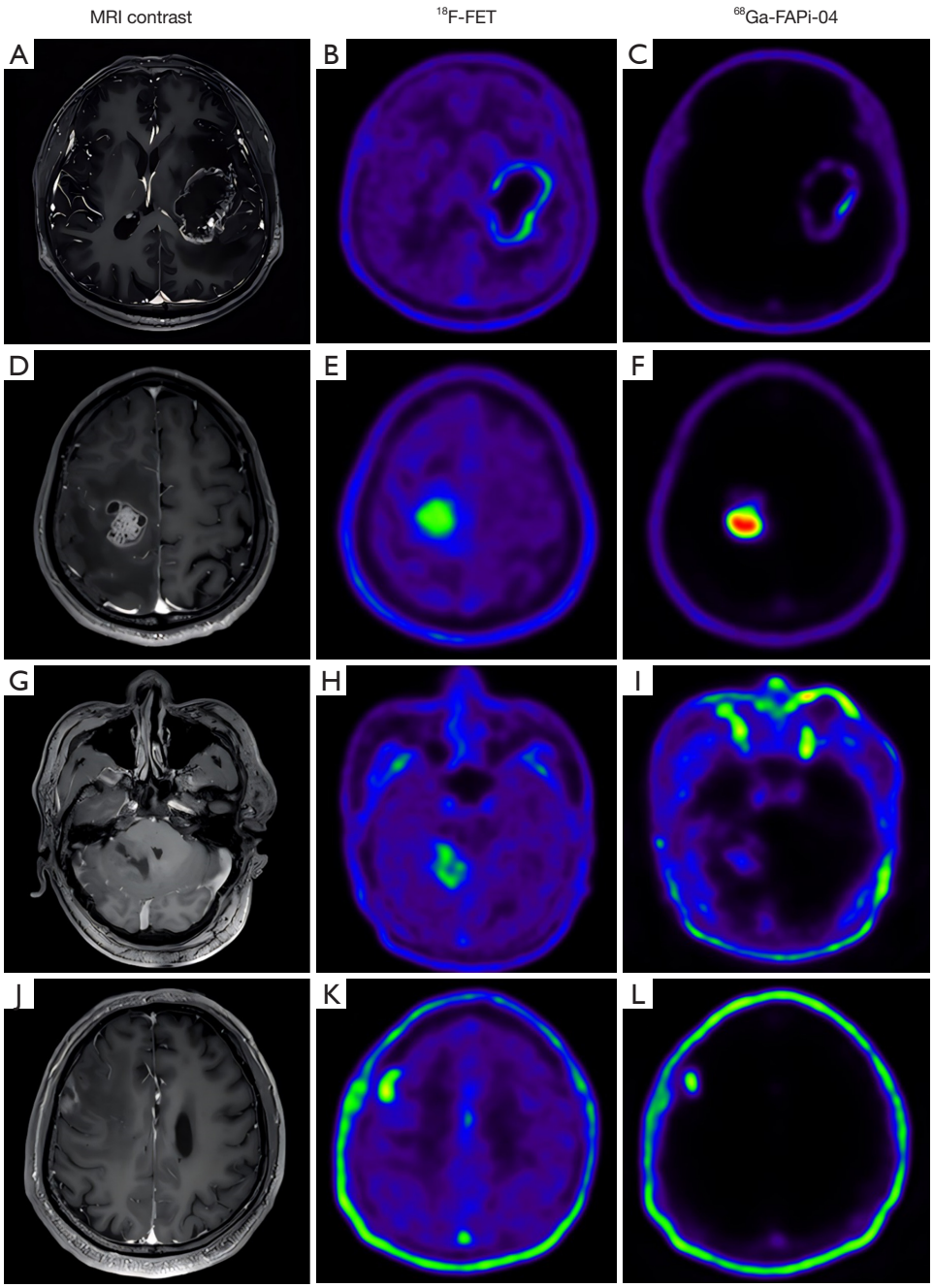

Figure 3 Typical MRI, ^{18}F-FET, and ^{68}Ga-FAPi-04 PET imaging of representative cases. (A-C) A 56-year-old male (No. 1) with WHO grade 4 left temporo-parietal glioblastoma IDH-wt. (D-F) A 58-year-old male (No. 15) with right fronto-parietal metastatic carcinoma. (G-I) A 35-year-old male (No. 21) with right cerebellar medulloblastoma. (J-L) A 46-year-old male (No. 13) with right frontal multifocal encephalomalacia. MRI, magnetic resonance image; ^{18}F-FET, fluoride-18 fluoroethyl-L-tyrosine; ^{68}Ga-FAPi-04, gallium-68 fibroblast activation protein inhibitor 04; PET, positron emission tomography; WHO, World Health Organization; IDH, isocitrate dehydrogenase; wt, wild type.

Table 2 Linear regression results of the ^{68}Ga-FAPi-04 and ^{18}F-FET PET semiquantitative parameters with different thresholds for lesion delineation

Delineation threshold	Parameter	Coefficient	P value	95% confidence interval	VIF
20% lesion FAPi SUVmax	MTV_{FAPi}:MTV_{FET} ratio	4.142	0.027*	0.572 to 7.712	5.02
	TLU_{FAPi}/TLU_{FET} ratio	−2.672	0.032*	−5.057 to −0.288	3.94
	TBRmax-FAPi	0.008	0.044*	0.000 to 0.016	2.75
	TBRmax-FET	−0.589	0.114	−1.347 to 0.169	1.65
30% lesion FAPi SUVmax	MTV_{FAPi}:MTV_{FET} ratio	5.484	0.052	−0.045 to 11.013	3.97
	TLU_{FAPi}:TLU_{FET} ratio	−3.095	0.067	−6.447 to 0.257	3.59
	TBRmax-FAPi	0.007	0.081	−0.001 to 0.015	2.45
	TBRmax-FET	−0.747	0.047*	−1.482 to −0.012	1.36
40% lesion FAPi SUVmax	MTV_{FAPi}:MTV_{FET} ratio	8.974	0.049*	0.044 to 17.903	3.28
	TLU_{FAPi}:TLU_{FET} ratio	−3.678	0.098	−8.174 to 0.818	2.87
	TBRmax-FAPi	0.007	0.082	−0.001 to 0.015	2.42
	TBRmax-FET	−0.601	0.104	−1.351 to 0.149	1.41
50% lesion FAPi SUVmax	MTV_{FAPi}:MTV_{FET} ratio	14.732	0.065	−1.131 to 30.596	2.82
	TLU_{FAPi}:TLU_{FET} ratio	−4.179	0.194	−10.857 to 2.500	2.49
	TBRmax-FAPi	0.006	0.116	−0.002 to 0.014	2.38
	TBRmax-FET	−0.428	0.279	−1.261 to 0.406	1.65

*, P<0.05. ^{68}Ga-FAPi-04, gallium-68 fibroblast activation protein inhibitor 04; ^{18}F-FET, fluoride 18 fluoroethyl-L-tyrosine; PET, positron emission tomography; VIF, variance inflation factor; FAPi, fibroblast activation protein inhibitor; SUVmax, maximal standardized uptake value; MTV, metabolic tumor volume; TLU, total lesion tracer uptake; TBRmax, maximal tumor-to-brain ratio; FET, fluoroethyl-L-tyrosine.

determine the efficacy of the PET parameters, with 1 noncancerous patient being excluded due to not meeting our research purpose. At a 20% FAPi lesion SUVmax threshold, the P value of the MTV_{FAPi}:MTV_{FET} ratio was 0.027 [95% confidence interval (CI): 0.572–7.712], the P value of the TLU_{FAPi}:TLU_{FET} ratio was 0.032 (95% CI: −5.057 to −0.288), and the P value of TBRmax-FAPi was 0.044 (95% CI: 0.000–0.016). At a 30% FAPi lesion SUVmax threshold, the P value of TBRmax-FET was 0.047 (95% CI: −1.482 to −0.012), while the P values of the MTV_{FAPi}:MTV_{FET} ratio, TLU_{FAPi}:TLU_{FET} ratio, and TBRmax-FAPi were 0.052 (95% CI: −0.045 to 11.013), 0.067 (95% CI: −6.447 to 0.257), and 0.081 (95% CI: −0.001 to 0.015), respectively. A 40% FAPi lesion SUVmax threshold, the P value of the MTV_{FAPi}:MTV_{FET} ratio was 0.049 (95% CI: 0.044–17.903), while the P values of TBRmax-FAPi and TLU_{FAPi}:TLU_{FET} were 0.082 (95% CI: −0.001 to 0.015) and 0.098 (95% CI: −8.174 to 0.818), respectively. At a 50% FAPi lesion SUVmax threshold, the P value of the MTV_{FAPi}:MTV_{FET} ratio was 0.065 (95% CI: −1.131 to 30.596). The detailed regression results details can be seen in *Table 2* and *Figure 4* and the scatter plot matrix of PET parameters and pathological diagnosis is provided in *Figure 5*.

FAP immunohistochemistry and ^{68}Ga-FAPi-04 PET imaging analysis

The FAP immunohistochemical scores from the two pathologists were in satisfactory agreement (ICC >0.92; P<0.001). In primary brain tumors, moderate FAP expression in the tumor stroma and peri-vascular areas could be observed in most of the patients with WHO grade 4 glioblastoma IDH-wt. Mild FAP expression was observed in the tumor stroma and perivascular areas in patients with WHO grade 4 and grade 3 astrocytoma IDH-mu. Scant-to-mild FAP expression was found in the tumor stromal areas of patients with low-grade gliomas including oligodendroglioma and ganglioglioma. Mild FAP

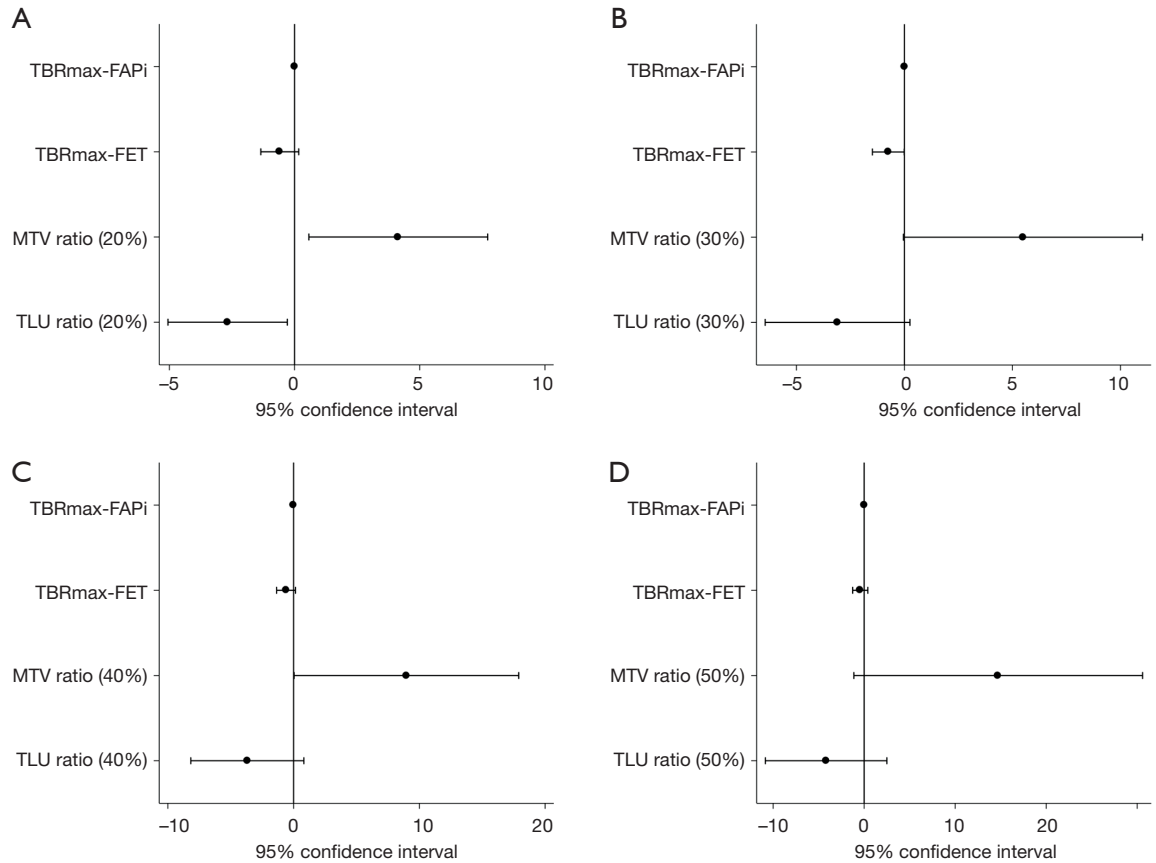

Figure 4 Linear regression results of the semiquantitative PET image parameters from 15 ^{68}Ga-FAPi-04-positive participants with intracranial tumor at 20% (A), 30% (B), 40% (C), and 50% (D) lesion SUVmax thresholds. TBRmax, maximal tumor-to-brain ratio; FAPi, fibroblast activation protein inhibitor; FET, fluoroethyl-L-tyrosine; MTV ratio, MTV_{FAPi}:MTV_{FET} ratio; MTV, metabolic tumor volume; TLU ratio, TLU_{FAPi}:TLU_{FET} ratio; TLU, total lesion tracer uptake; PET, positron emission tomography; ^{68}Ga-FAPi-04, gallium-68 fibroblast activation protein inhibitor 04; SUVmax, maximal standardized uptake value.

expression was found in the tumor stroma of the patient with medulloblastoma but not in the perivascular region. In brain metastasis, significant tumor stroma, perivascular, and small vessel epithelial expression were found. In patient 13, who had a noncancerous lesion, moderate FAP expression was present in the stromal cells in inflamed regions, the perivascular region, the small-vessel epithelium, and the gliotic region; meanwhile, mild FAP expression was observed in the small vessel epithelium and gliotic region in patient 10 (*Figure 6*).

The lesion median SUVmax was 0.4 (range, 0.2–1.3), 4.0 (range, 3.2–5.8), and 10.4 (range, 8.9–19.1) in patients with an FAP immunohistochemical score from 1 to 3, respectively. The lesion FAPi SUVmax was significantly correlated with FAP immunohistochemical score (r^2=0.70; P<0.001) (*Figure 2*).

Discussion

Despite there being distinct characteristics of FAP expression across a wide range of carcinomas, limited evidence exists regarding its expression patterns in intracranial tumors. Our study found there to be heterogeneous uptake of ^{68}Ga-FAPi-04 across our cohort, with generally significant uptake noted in patients with brain metastasis, glioblastoma, and medulloblastoma. The immunohistochemical results showed varied FAP expression patterns in primary tumors, brain metastasis, and noncancerous disease. In FAPi-positive intracranial tumors, the MTV_{FAPi}:MTV_{FET} ratio, a semiquantitative parameter which can be used to reflect the quantification results of CAFs activity in tumor parenchyma, has shown promising differential potential in intracranial tumors.

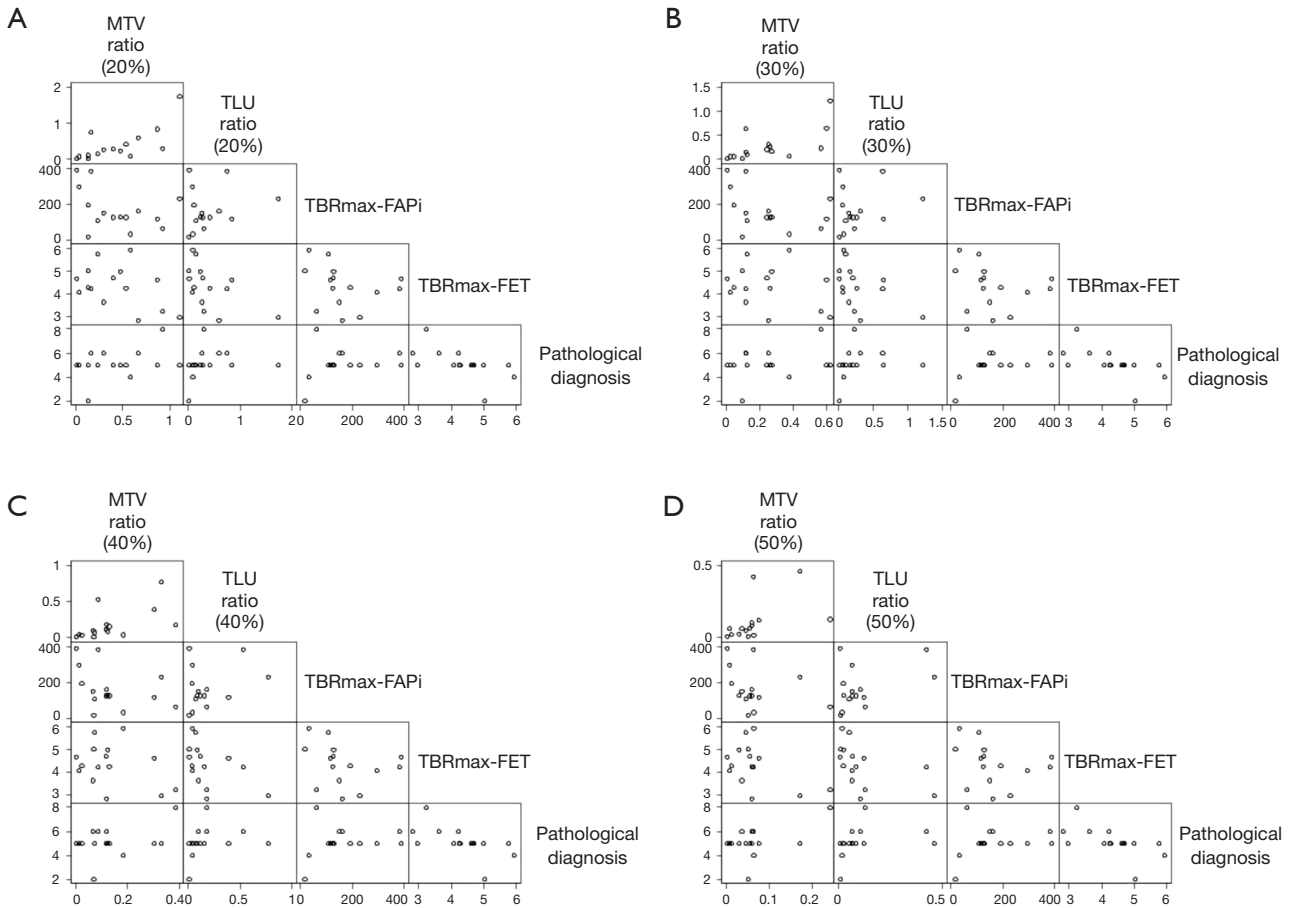

Figure 5 Scatter plot matrix from the MTV_{FAPi}:MTV_{FET} ratio, TLU_{FAPi}:TLU_{FET} ratio, TBRmax-FAPi, TBRmax-FET, and pathological diagnosis with 20% (A), 30% (B), 40% (C), and 50% (D) lesion SUVmax thresholds. MTV ratio, MTV_{FAPi}:MTV_{FET} ratio; MTV, metabolic tumor volume; TLU ratio, TLU_{FAPi}:TLU_{FET} ratio; TLU, total lesion tracer uptake; TBRmax, maximal tumor-to-brain ratio; FAPi, fibroblast activation protein inhibitor; FET, fluoroethyl-L-tyrosine; SUVmax, maximal standardized uptake value.

Limited research in the FAP of gliomas suggests there to be increased FAPi uptake in high-grade gliomas (21). Other analysis indicates that FAPi uptake in high-grade gliomas partly correlates with the tumor perfusion but not with the cell density of these gliomas (23). Our study expanded the scope to an intracranial tumor cohort, and FAP expression status was generally associated with tumor malignancy degree, in accordance with previous investigations. Immunohistochemical analysis indicated that the differences of FAP expression were mainly present in the areas of the TME, including perivascular region. These patchy- and spot-like FAP expressions in intracranial tumor stroma correlated with ^{68}Ga-FAPi-04 uptake. Based on this, we hypothesized that FAP expression in perivascular stromal region is associated with tumor lesion perfusion, while the cellular density status of the intracranial tumor is not correlated with its FAP expression status, which results in the absence of relationship between FAPi uptake and the apparent diffusion coefficient of the tumor.

Radio-labeled amino acid tracers have satisfactory diagnostic efficacy in brain tumors (9,24). ^{18}F-FET PET imaging can well delineate a wide range of intracranial tumors in our cohort, even some small lesions. However, TME cell-targeting tracers can offer new possibilities in evaluating the heterogeneities of intracranial tumors in addition to tumor cell-targeted imaging. The TME consists of a range of benign cells that interact with tumor cells, influencing growth, migration, and recurrence (25-27). FAP expression has been observed in most epithelial neoplasms (28). Due to unique classification and characteristics of central

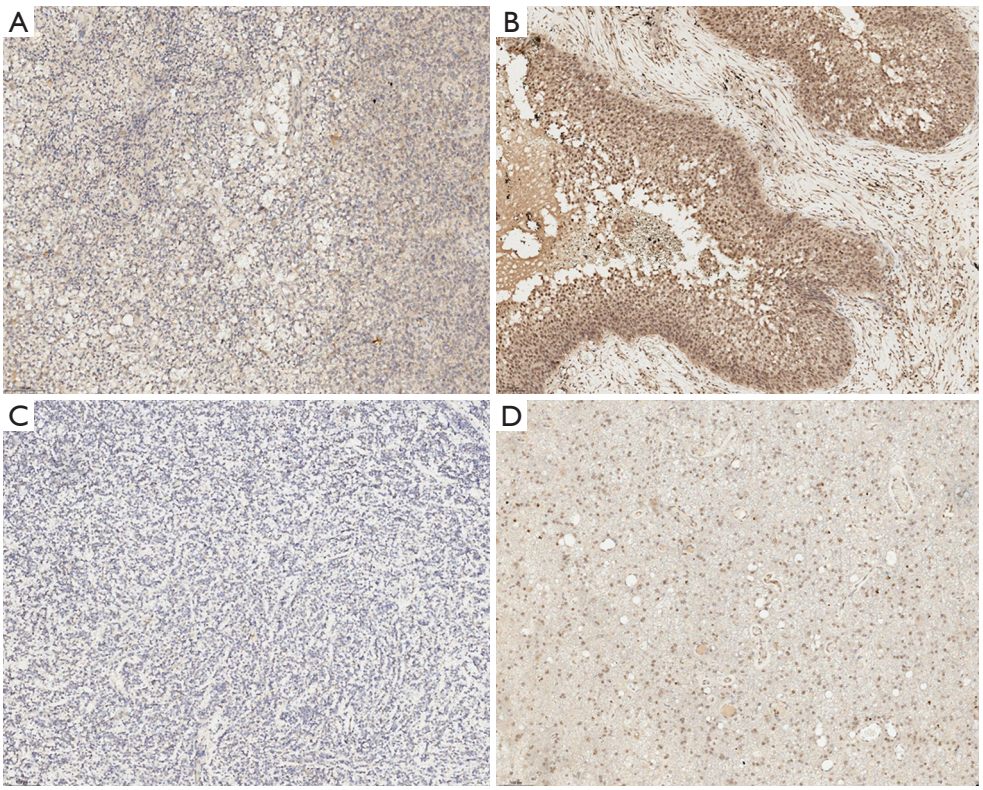

Figure 6 Typical case illustrations of FAP immunohistochemical staining imaging (original magnification, 200×). (A) WHO grade 4 glioblastoma IDH-wt (No. 1) with moderate FAP expression in tumor stroma and perivascular region. (B) Metastatic carcinoma (No. 15) with significant FAP expression in tumor stroma, perivascular region, and small-vessel epithelial tissue. (C) Medulloblastoma (No. 21) with mild FAP expression in the tumor stroma. (D) Multifocal encephalomalacia (No. 13) with moderate FAP expression in stromal cells in inflamed regions, perivascular region, small-vessel epithelial tissue, and gliotic region. FAP, fibroblast activation protein; WHO, World Health Organization; IDH, isocitrate dehydrogenase; wt, wild type.

nervous system (29), moderate FAP expression was present in most of the patients with WHO grade 4 glioblastoma IDH-wt in our cohort. These patients typically have a very poor prognosis, and the expression pattern of FAP could provide valuable data for future FAP-targeted theranostic methods, serving as a complement to classical treatment procedures.

Lesion delineation is vital for devising a treatment plan. Radio-labeled amino acid tracer imaging could be used to outline lesions (30). There is evidence supporting the potential of FAP-targeted imaging in the differentiation and delineation of intracranial malignant tumors. It is reasonable to suggest that FAPi imaging can complement current imaging protocols for intracranial malignancies. Besides FAPi imaging, comprehensive analysis of anatomic MRI and amino acid PET imaging are necessary to exclude occasional benign lesions with FAP expression. The costs of FAP-targeted imaging are similar to those of widely clinically used tracers, and the potential benefits of the noninvasive malignant degree recognition and evidence-guided treatment planning via FAP-targeted imaging should be considered.

There is currently no standard for brain lesion delineation in FAP-targeted imaging. Considering the characteristics of brain tumors and FAP expression status in normal brain background, we applied 20% lesion SUVmax as the threshold for the initial observation in ^{68}Ga-FAPi-04 PET analysis. Further observations were investigated with 30%, 40%, and 50% of the lesion SUVmax being used as thresholds. This strategy was employed to control the influence of delineation fluctuation owing to the extremely low uptake of the brain background. Given the significant tumor-to-brain ratio of FAPi uptake, a 20% isocontour volumetric threshold is reasonable for lesion delineation.

There are growing amount of studies on ^{68}Ga-FAPi uptake in noncancerous diseases including autoimmune disease, cardiovascular disease, wound healing (31-34). The results from this varied research indicates the potential of FAPi in the molecular imaging of inflammation. In our cohort, the participants with noncancerous lesions also had ^{68}Ga-FAPi-04 uptake, suggesting that caution should be taken in the diagnosis of positive ^{68}Ga-FAPi-04 lesions. In classical semiquantitative parameters, characteristic time-activity curve patterns from dynamic ^{18}F-FET PET imaging could help to differentiate between glioma subtypes and exclude noncancerous lesions. Other imaging parameters should be considered for participants for whom diagnosis is unclear.

Our study involved certain limitations which should be addressed. First, our head-to-head study included a relatively small size, and the results of this exploratory investigation need to be further confirmed with a more robust patient cohort. Second, this initial study mainly concentrated on cohort ^{68}Ga-FAPi-04 and ^{18}F-FET PET/CT imaging analysis, the combination of anatomic MRI parameters with those examined in our study will complement these results. More investigations including histopathological validation of the different FAPi imaging threshold-based lesion delineations and imaging quantification analysis combined with anatomic MRI features will doubtlessly contribute to furthering our understanding of the effects of CAFs in the intracranial TME.

Conclusions

Our study found heterogeneities in ^{68}Ga-FAPi-04 uptake in this intracranial tumor cohort, with tumors with greater malignancy generally having an elevated FAP expression, although the difference between the primary brain tumor, brain metastasis, and noncancerous disease were statistically nonsignificant. Immunohistochemical analysis revealed a diversity of FAP expression patterns. For intracranial tumor patients with positive ^{68}Ga-FAPi-04 uptake, the MTV_{FAPi}:MTV_{FET} ratio demonstrated potential in differentiating between various intracranial tumors, suggesting that the interactions between intracranial tumor parenchyma and CAF cells in the TME are distinct across various types of tumor genesis.

Acknowledgments

We appreciate the kind support from pharmacists, nurses, and technicians of the Department of Nuclear Medicine & PET Center; and pathologists Haixia Cheng and Jingjing Zhu from the Department of Pathology, Huashan Hospital, Fudan University.

Funding: This work was supported by the Science and Technology Commission of Shanghai Municipality (grant Nos. 18411952100 and 2018SHZDZX01) and Zhang Jiang Lab.

Footnote

Conflicts of Interest: All authors have completed the ICMJE uniform disclosure form (available at https://qims.amegroups.com/article/view/10.21037/qims-24-82/coif). The authors have no conflicts of interest to declare.

Ethical Statement: The authors are accountable for all aspects of the work in ensuring that questions related to the accuracy or integrity of any part of the work are appropriately investigated and resolved. This study was conducted according to the Declaration of Helsinki (as revised in 2013). Ethical approval of our previously written study protocol and consequent analytical design was obtained from Ethics Committee of Huashan Hospital, Fudan University (No. 2021-891), and informed consent was obtained from all individual participants.

References

1. Kim H, Zheng S, Amini SS, Virk SM, Mikkelsen T, Brat DJ, et al. Whole-genome and multisector exome sequencing of primary and post-treatment glioblastoma reveals patterns of tumor evolution. Genome Res 2015;25:316-27.
2. Sottoriva A, Spiteri I, Piccirillo SG, Touloumis A, Collins VP, Marioni JC, Curtis C, Watts C, Tavaré S. Intratumor heterogeneity in human glioblastoma reflects cancer evolutionary dynamics. Proc Natl Acad Sci U S A

2013;110:4009-14.
3. Bhat KPL, Balasubramaniyan V, Vaillant B, Ezhilarasan R, Hummelink K, Hollingsworth F, et al. Mesenchymal differentiation mediated by NF-κB promotes radiation resistance in glioblastoma. Cancer Cell 2013;24:331-46.
4. Quail DF, Joyce JA. Microenvironmental regulation of tumor progression and metastasis. Nat Med 2013;19:1423-37.
5. Naba A, Clauser KR, Hoersch S, Liu H, Carr SA, Hynes RO. The matrisome: in silico definition and in vivo characterization by proteomics of normal and tumor extracellular matrices. Mol Cell Proteomics 2012;11:M111.014647.
6. Poetsch N, Woehrer A, Gesperger J, Furtner J, Haug AR, Wilhelm D, Widhalm G, Karanikas G, Weber M, Rausch I, Mitterhauser M, Wadsak W, Hacker M, Preusser M, Traub-Weidinger T. Visual and semiquantitative 11C-methionine PET: an independent prognostic factor for survival of newly diagnosed and treatment-naïve gliomas. Neuro Oncol 2018;20:411-9.
7. Katsanos AH, Alexiou GA, Fotopoulos AD, Jabbour P, Kyritsis AP, Sioka C. Performance of 18F-FDG, 11C-Methionine, and 18F-FET PET for Glioma Grading: A Meta-analysis. Clin Nucl Med 2019;44:864-9.
8. Paprottka KJ, Kleiner S, Preibisch C, Kofler F, Schmidt-Graf F, Delbridge C, Bernhardt D, Combs SE, Gempt J, Meyer B, Zimmer C, Menze BH, Yakushev I, Kirschke JS, Wiestler B. Fully automated analysis combining [18F]-FET-PET and multiparametric MRI including DSC perfusion and APTw imaging: a promising tool for objective evaluation of glioma progression. Eur J Nucl Med Mol Imaging 2021;48:4445-55.
9. Albert NL, Weller M, Suchorska B, Galldiks N, Soffietti R, Kim MM, la Fougère C, Pope W, Law I, Arbizu J, Chamberlain MC, Vogelbaum M, Ellingson BM, Tonn JC. Response Assessment in Neuro-Oncology working group and European Association for Neuro-Oncology recommendations for the clinical use of PET imaging in gliomas. Neuro Oncol 2016;18:1199-208.
10. Nawashiro H, Otani N, Shinomiya N, Fukui S, Ooigawa H, Shima K, Matsuo H, Kanai Y, Endou H. L-type amino acid transporter 1 as a potential molecular target in human astrocytic tumors. Int J Cancer 2006;119:484-92.
11. Habermeier A, Graf J, Sandhöfer BF, Boissel JP, Roesch F, Closs EI. System L amino acid transporter LAT1 accumulates O-(2-fluoroethyl)-L-tyrosine (FET). Amino Acids 2015;47:335-44.
12. Liu T, Han C, Wang S, Fang P, Ma Z, Xu L, Yin R. Cancer-associated fibroblasts: an emerging target of anti-cancer immunotherapy. J Hematol Oncol 2019;12:86.
13. Scanlan MJ, Raj BK, Calvo B, Garin-Chesa P, Sanz-Moncasi MP, Healey JH, Old LJ, Rettig WJ. Molecular cloning of fibroblast activation protein alpha, a member of the serine protease family selectively expressed in stromal fibroblasts of epithelial cancers. Proc Natl Acad Sci U S A 1994;91:5657-61.
14. Kalluri R. The biology and function of fibroblasts in cancer. Nat Rev Cancer 2016;16:582-98.
15. Ao M, Brewer BM, Yang L, Franco Coronel OE, Hayward SW, Webb DJ, Li D. Stretching fibroblasts remodels fibronectin and alters cancer cell migration. Sci Rep 2015;5:8334.
16. Sollini M, Kirienko M, Gelardi F, Fiz F, Gozzi N, Chiti A. State-of-the-art of FAPI-PET imaging: a systematic review and meta-analysis. Eur J Nucl Med Mol Imaging 2021;48:4396-414.
17. Kratochwil C, Flechsig P, Lindner T, Abderrahim L, Altmann A, Mier W, Adeberg S, Rathke H, Röhrich M, Winter H, Plinkert PK, Marme F, Lang M, Kauczor HU, Jäger D, Debus J, Haberkorn U, Giesel FL. (68)Ga-FAPI PET/CT: Tracer Uptake in 28 Different Kinds of Cancer. J Nucl Med 2019;60:801-5.
18. Loktev A, Lindner T, Mier W, Debus J, Altmann A, Jäger D, Giesel F, Kratochwil C, Barthe P, Roumestand C, Haberkorn U. A Tumor-Imaging Method Targeting Cancer-Associated Fibroblasts. J Nucl Med 2018;59:1423-9.
19. Backhaus P, Burg MC, Roll W, Büther F, Breyholz HJ, Weigel S, Heindel W, Pixberg M, Barth P, Tio J, Schäfers M. Simultaneous FAPI PET/MRI Targeting the Fibroblast-Activation Protein for Breast Cancer. Radiology 2022;302:39-47.
20. Spektor AM, Gutjahr E, Lang M, Glatting FM, Hackert T, Pausch T, Tjaden C, Schreckenberger M, Haberkorn U, Röhrich M. Immunohistochemical FAP Expression Reflects (68)Ga-FAPI PET Imaging Properties of Low- and High-Grade Intraductal Papillary Mucinous Neoplasms and Pancreatic Ductal Adenocarcinoma. J Nucl Med 2024;65:52-8.
21. Röhrich M, Loktev A, Wefers AK, Altmann A, Paech D, Adeberg S, Windisch P, Hielscher T, Flechsig P, Floca R, Leitz D, Schuster JP, Huber PE, Debus J, von Deimling A, Lindner T, Haberkorn U. IDH-wildtype glioblastomas and grade III/IV IDH-mutant gliomas show elevated tracer uptake in fibroblast activation protein-specific PET/CT. Eur J Nucl Med Mol Imaging 2019;46:2569-80.

22. Henry LR, Lee HO, Lee JS, Klein-Szanto A, Watts P, Ross EA, Chen WT, Cheng JD. Clinical implications of fibroblast activation protein in patients with colon cancer. Clin Cancer Res 2007;13:1736-41.
23. Röhrich M, Floca R, Loi L, Adeberg S, Windisch P, Giesel FL, Kratochwil C, Flechsig P, Rathke H, Lindner T, Loktev A, Schlemmer HP, Haberkorn U, Paech D. FAP-specific PET signaling shows a moderately positive correlation with relative CBV and no correlation with ADC in 13 IDH wildtype glioblastomas. Eur J Radiol 2020;127:109021.
24. Placone AL, Quiñones-Hinojosa A, Searson PC. The role of astrocytes in the progression of brain cancer: complicating the picture of the tumor microenvironment. Tumour Biol 2016;37:61-9.
25. Matias D, Balça-Silva J, da Graça GC, Wanjiru CM, Macharia LW, Nascimento CP, Roque NR, Coelho-Aguiar JM, Pereira CM, Dos Santos MF, Pessoa LS, Lima FRS, Schanaider A, Ferrer VP; Moura-Neto V. Microglia/Astrocytes-Glioblastoma Crosstalk: Crucial Molecular Mechanisms and Microenvironmental Factors. Front Cell Neurosci 2018;12:235.
26. Venkatesh HS, Tam LT, Woo PJ, Lennon J, Nagaraja S, Gillespie SM, Ni J, Duveau DY, Morris PJ, Zhao JJ, Thomas CJ, Monje M. Targeting neuronal activity-regulated neuroligin-3 dependency in high-grade glioma. Nature 2017;549:533-7.
27. Mona CE, Benz MR, Hikmat F, Grogan TR, Lueckerath K, Razmaria A, Riahi R, Slavik R, Girgis MD, Carlucci G, Kelly KA, French SW, Czernin J, Dawson DW, Calais J. Correlation of (68)Ga-FAPi-46 PET Biodistribution with FAP Expression by Immunohistochemistry in Patients with Solid Cancers: Interim Analysis of a Prospective Translational Exploratory Study. J Nucl Med 2022;63:1021-6.
28. Law I, Albert NL, Arbizu J, Boellaard R, Drzezga A, Galldiks N, la Fougère C, Langen KJ, Lopci E, Lowe V, McConathy J, Quick HH, Sattler B, Schuster DM, Tonn JC, Weller M. Joint EANM/EANO/RANO practice guidelines/SNMMI procedure standards for imaging of gliomas using PET with radiolabelled amino acids and [18F]FDG: version 1.0. Eur J Nucl Med Mol Imaging 2019;46:540-57.
29. Unterrainer M, Vettermann F, Brendel M, Holzgreve A, Lifschitz M, Zähringer M, Suchorska B, Wenter V, Illigens BM, Bartenstein P, Albert NL. Towards standardization of (18)F-FET PET imaging: do we need a consistent method of background activity assessment? EJNMMI Res 2017;7:48.
30. Louis DN, Perry A, Wesseling P, Brat DJ, Cree IA, Figarella-Branger D, Hawkins C, Ng HK, Pfister SM, Reifenberger G, Soffietti R, von Deimling A, Ellison DW. The 2021 WHO Classification of Tumors of the Central Nervous System: a summary. Neuro Oncol 2021;23:1231-51.
31. Luo Y, Pan Q, Yang H, Peng L, Zhang W, Li F. Fibroblast Activation Protein-Targeted PET/CT with (68)Ga-FAPI for Imaging IgG4-Related Disease: Comparison to (18)F-FDG PET/CT. J Nucl Med 2021;62:266-71.
32. Qin C, Yang L, Ruan W, Shao F, Lan X. Immunoglobulin G4-Related Sclerosing Cholangitis Revealed by 68Ga-FAPI PET/MR. Clin Nucl Med 2021;46:419-21.
33. Kessler L, Kupusovic J, Ferdinandus J, Hirmas N, Umutlu L, Zarrad F, Nader M, Fendler WP, Totzeck M, Wakili R, Schlosser T, Rassaf T, Rischpler C, Siebermair J. Visualization of Fibroblast Activation After Myocardial Infarction Using 68Ga-FAPI PET. Clin Nucl Med 2021;46:807-13.
34. Zhou Y, Yang X, Liu H, Luo W, Liu H, Lv T, Wang J, Qin J, Ou S, Chen Y. Value of [68Ga]Ga-FAPI-04 imaging in the diagnosis of renal fibrosis. Eur J Nucl Med Mol Imaging 2021;48:3493-501.

Cite this article as: Hua T, Chen M, Fu P, Zhou W, Zhao W, Li M, Zuo C, Guan Y, Xu H. Heterogeneity of fibroblast activation protein expression in the microenvironment of an intracranial tumor cohort: head-to-head comparison of gallium-68 FAP inhibitor-04 (^{68}Ga-FAPi-04) and fluoride-18 fluoroethyl-L-tyrosine (^{18}F-FET) in positron emission tomography-computed tomography imaging. Quant Imaging Med Surg 2024;14(7):4450-4463. doi: 10.21037/qims-24-82

